SSOH and HSSO Radicals: An Experimental and Theoretical Study of $[S_2OH]^{0/+/-}$ Species

Giulia de Petris,*,† Marzio Rosi,‡ and Anna Troiani†

Dipartimento di Studi di Chimica e Tecnologia delle Sostanze Biologicamente Attive, Università "La Sapienza" Piazzale Aldo Moro 5-00185 Rome, Italy, and Dipartimento di Ingegneria Civile ed Ambientale - Sezione Tecnologie Chimiche e Materiali per l'Ingegneria, ISTM-CNR - Università di Perugia, Via Duranti, I-06131, Perugia, Italy

Received: March 13, 2007; In Final Form: April 23, 2007

New radicals containing sulfur−sulfur bonds are detected in the gas phase: disulfur hydroxide SSOH and thiosulfenoxide HSSO, stable toward dissociation by ca. 50 and 40 kcal mol^{-1}, respectively. Energetic, structural features and fragmentation pathways of these $[S_2OH]$ radicals and their charged species $[S_2OH]^+$ and $[S_2OH]^-$ are experimentally and computationally investigated by mass spectrometric techniques and ab initio calculations. $[S_2OH]^+$ is obtained by various ion−molecule reactions leading to S_2O protonated on the oxygen and end-sulfur atoms, whose proton affinity is computed at different levels of theory. The first detection of $[S_2OH]^-$, the conjugate base of the oxatrisulfane HSSOH, is also reported.

Introduction

The rich inventory of sulfur compounds containing hydrogen and oxygen atoms displays only a few known $[H, S_n, O]^{0/+/-}$ species. The HSO and SOH radicals and their cations and anions are the well-known, most simple species of this family.[1] Adams et al. suggested the existence of the SSOH radical as a neutral product of the reaction of S_2^+ with some organic acids and alcohols.[2] However, with $n = 2$, only the cation has been observed on a few occasions as a fragment in mass spectra of sulfur species.[3] So far $[H, S_2, O]$ and $[H, S_2, O]^-$ are still unknown species.

As a continuation of our interest in sulfur-rich compounds,[4] in this work we report the first experimental detection of disulfur hydroxide SSOH and thiosulfenoxide HSSO. The study was performed by mass spectrometric techniques augmented by theoretical calculations of the relevant species, henceforth formally denoted $[S_2OH]^{0/+/-}$. The aim of the study is (i) to generate and structurally characterize isomeric cations $[S_2OH]^+$ using different ion−molecule reactions, (ii) to generate SSOH, investigate its isomerization to HSSO, and determine the minimum lifetime, (iii) to generate the corresponding $[S_2OH]^-$ anions, the conjugate bases of the oxatrisulfane HS_2OH.[5] In this contest, the proton affinity of the electron-rich S_2O was computed at different levels of theory and examined in relation to the analogous molecules O_3 and SO_2.

The title species prove to be the simplest $[H, S_n, O]$ compounds containing sulfur−sulfur bonds, whose potential interest as building blocks in organic and biological molecules adds to their fundamental relevance. SSOH is a sulfur analogue of O_3H and SO_2H, the suggested intermediates of the atmospherically relevant reactions $OH(v) + O_2 \rightarrow H + O_3$ and $OH + SO \rightarrow H + SO_2$.[6,7] The existence of SSOH as a stable species in the gas phase may encourage the study of the reaction $OH + S_2 \rightarrow H + S_2O$ and of the possible role of S_2OH radicals in sulfur-rich planetary atmospheres and sulfur-doped flames.[8−9]

* To whom correspondence should be addressed. E-mail: giulia.depetris@uniromal.it.
† Università "La Sapienza".
‡ Università di Perugia.

Experimental Section

A. Mass Spectrometric Methods. All experiments were performed using a modified ZABSpec oa-TOF instrument (VG Micromass) of EBE-TOF configuration, where E and B stand for electric and magnetic sectors, respectively, and TOF stands for orthogonal time-of-flight mass spectrometer.[10] The instrument was fitted with a EI-CI ion source, a gas cell located in the first field-free region, and two pairs of gas cells located after the magnet in the second field-free region and in the TOF sector, respectively. Typical operating conditions were as follows: accelerating voltage, 8 keV; source temperature, 433 K; repeller voltage, 0 V; emission current, 1 mA; nominal electron energy, 50 eV; and source pressure ranging from ca. 0.02 to 0.2 Torr, as read inside the source block by a Magnehelic differential pressure gauge. High-resolution CI mass spectra were recorded at 15000 full width at half maximum (fwhm). The CAD/TOF spectra were recorded at 0.8 keV in the TOF sector of the instrument, after mass and energy selection of the ion. The 8 keV CAD spectra were recorded with fully open source and energy slits. Helium was utilized as the target gas in the CAD experiments; it was admitted into the collision cell at such a pressure to achieve 80% transmittance.

The neutralization−reionization (NR) experiments[11] were performed at high (8 keV) and low (0.8 keV) collision energy, in the pair of cells located in the second field-free region and in the TOF sector of the instrument, respectively. In the first collision cell, the mass-selected parent cation undergoes a vertical, one-electron reduction by collision with Xe. All ions are removed at the exit of the cell by a pair of high-voltage deflecting electrodes. A beam containing only neutrals enters the second cell, where it is reionized undergoing a vertical, one-electron oxidation by collision with O_2 (high-energy $^+NR^+$) or Ar (low-energy $^+NR^+$). No signal was obtained by switching the deflector on without the reionizing gas. The neutral beam may contain fragments and intact neutral molecules, the latter are reionized provided that they survive for the time necessary to travel from the first to the second cell. The detection of intact neutral species is proved by detection of a "recovery" peak at the same m/z ratio as the original ion. In $^+NR^-$ experiments,

10.1021/jp072025r CCC: $37.00
Published on Web 06/20/2007

the neutrals undergo a vertical, one-electron reduction by collision with Xe. In charge reversal ($^+CR^-$) experiments the parent ion undergoes a two-electron reduction by collision with Xe in only one collision cell. All gases were admitted into the cells at such a pressure to achieve a beam transmittance of 80%, under near-single collision conditions. All NR spectra were averaged over 100 acquisitions to improve the signal-to-noise ratio. The recovery peaks of the high-energy $^+NR^+$ and $^+NR^-$ spectra were analyzed in the TOF sector (He, collision gas).

B. Materials. The chemicals were research-grade products with the following stated purity: HgS (Aldrich, 99.999 mol %), elemental sulfur-S (Aldrich, 99.998 mol %), elemental sulfur-^{34}S (Aldrich, 99.5% ^{34}S atoms), and $H_2{}^{18}O$ (Isotec, 97% ^{18}O atoms). All other chemicals were research-grade products with a stated purity in excess of 99.95 mol %. Elemental sulfur and HgS were introduced through a direct insertion probe and heated in vacuo at temperatures not exceeding 400 and 500 K, respectively. Note that slightly different spectra from that reported in Figure 4B were obtained by heating HgS at $T >$ 500 K (showing small signals corresponding to S_3^+ and S_4^+). S_2O was prepared in situ by reaction of thionyl chloride $SOCl_2$ and silver sulfide Ag_2S heated in a pyrex tube to 423 K.[12]

C. Computational Methods. Density functional theory, using the hybrid B3LYP functional, was used to localize the stationary points of the investigated systems and to evaluate the vibrational frequencies.[13] Although it is well-known that density functional methods using non-hybrid functionals sometimes tend to overestimate bond lengths,[14] hybrid functionals such as B3LYP usually provide geometrical parameters in excellent agreement with the experiment.[15] Single-point energy calculations at the optimized geometries were performed using the coupled-cluster single and double excitation method with a perturbational estimate of the triple excitation [CCSD(T)] approach, to include extensive correlation contributions.[16] Transition states were located using the synchronous transit−guided quasi-Newton method of Schlegel and co-workers.[17] The correlation-consistent valence-polarized set aug-cc-pVTZ, developed by Dunning and co-workers, was used. [18] A tight d function with exponent 2.457 for S and 6.942 for O was added to this basis set, as suggested by Bauschlicher and Partridge.[19] It is known that ab initio calculations with both split-valence and correlation-consistent basis sets may give an inaccurate description of structures and energies of some sulfur species.[20] Moreover, isomerization and dissociation energies can be overestimated in systems having multiconfigurational character.[21] We have compared the differences between the computed dissociation limits with the known experimental values. They generally agree within 2 kcal mol^{-1} whereas a larger deviation is observed in some reactions involving $S_2O^{+/0/-}$, where the best results are achieved with the CBS-Q method.[22] As an example, the experimental $\Delta H°$ of the reaction $S_2 + OH \rightarrow S_2O + H$ is −1.1 kcal mol^{-1},[23] and the computed $\Delta H°$ values are 8.9 (B3LYP), 4.6 (CCSD(T)), and 0.7 (CBS-Q) kcal mol^{-1}, respectively. Likewise, the experimental $\Delta H°$ value of the reaction $SH^- + SO \rightarrow S_2O^- + H$ is 14.6 kcal mol^{-1},[23] and the computed $\Delta H°$ values are 18.0 (B3LYP), 17.7 (CCSD(T)), and 13.3 (CBS-Q) kcal mol^{-1}, respectively. Intrinsic reaction coordinate (IRC) calculations[24] were performed at the B3LYP level of theory for selected transition structures, to ascertain that they connect the identified reactants and products. The analysis of the transition states was performed using the program Molekel.[25] Zero-point energy corrections evaluated at the B3LYP level were added to the CCSD(T) energies. The 0 K total energies of the species of interest were corrected to 298 K by adding translational, rotational, and vibrational contributions. All calculations were performed using Gaussian 03.[26]

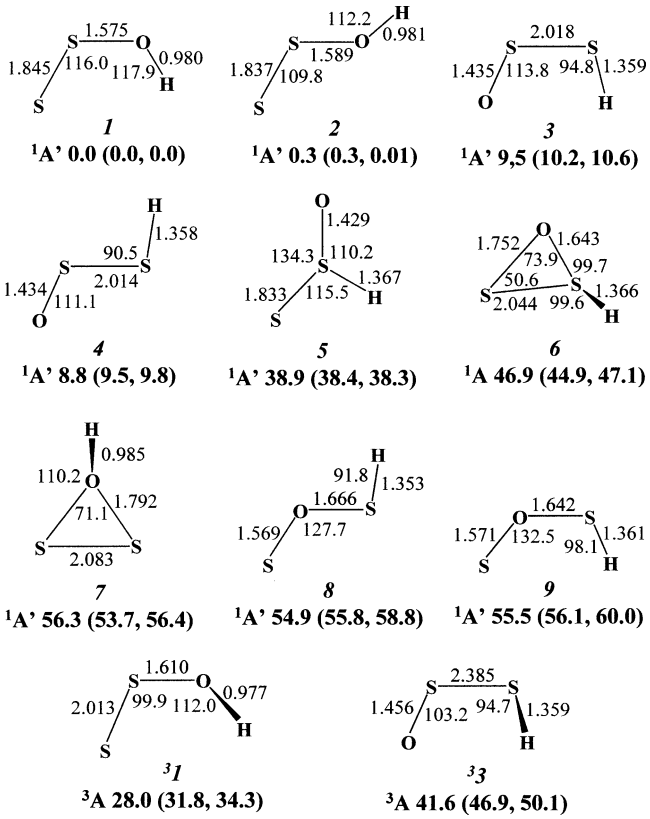

Figure 1. B3LYP optimized geometries and relative energies (kcal mol^{-1}) at 298 K of $[S_2OH]^+$ ions, shown in parentheses are CCSD(T) and CBS-Q relative energies.

Results and Discussion

Ab Initio Structures and Energies. First we examine the computational results as a framework for discussing the energetic and structural features of the ionic and neutral species detected in this study. With the exception of one SCF study of protonated S_2O,[27] to our knowledge, no previous theoretical studies exist.

$[S_2OH]^+$. The most stable isomer is the cis $SSOH^+$ ion **1** (Figure 1). The trans isomer **2** lies only 0.3 kcal mol^{-1} higher in energy. The optimized geometry and the Mulliken population analysis suggest an almost double S−S bond and a single S−O bond. The positive charge is mostly localized on the central sulfur atom, and the single S−O bond accounts for the low barrier (6.9 kcal mol^{-1}) for the cis−trans isomerization (Table 1). At higher energy, we located the $HSSO^+$ ions **3** and **4**, where the sulfur atom coordinated to the oxygen bears most of the positive charge (+1.0 e), and the other sulfur atom also carries a not negligible positive charge (+0.2 e). Moreover, a significant negative charge (−0.5 e) is localized on the oxygen atom. This charge distribution and the optimized geometry imply the presence of a partial double S−O bond. The S−S bond is not a pure single bond, which explains the presence of a barrier (18.0 kcal mol^{-1}) for the cis−trans isomerization (Table 1). The $SSOH^+$ and $HSSO^+$ ions were found to isomerize through the two cis forms **1** and **3**, by overcoming a barrier of 36.9 kcal mol^{-1} that lies below the lowest-energy dissociations of $SSOH^+$ and $HSSO^+$ (Table 1). At higher energy with respect to ions **1**−**4**, we found the $HS(S)O^+$ ion **5**, two nonplanar ring species (**6** and **7**) and two $SOSH^+$ ions (**8** and **9**). A high barrier characterizes the **4** → **5** isomerization (54.8 kcal mol^{-1}), and

TABLE 1: Energy Changes and Barrier Heights (kcal mol^{-1}, 298 K) Computed at the B3LYP/aug-cc-pVTZ+d, CCSD(T)/aug-cc-pVTZ+d, and CBS-Q Levels of Theory for Selected Dissociation and Isomerization Processes of S_2OH^+

	ΔH^a			barrier height	
process	B3LYP	CCSD(T)	CBS-Q	B3LYP	CCSD(T)
1 → **2**	0.3	0.3	0.01	6.8	6.9
3 → **4**	-0.7	-0.7	-0.8	19.5	18.0
1 → **3**	9.5	10.2	10.6	38.7	36.9
4 → **5**	30.1	28.9	28.5	56.9	54.8
^{3}**1** → ^{3}**3**	13.6	15.1	15.8	36.1	38.5
1 → $S_2^+ + OH$	69.6	70.4	74.9		
1 → $SOH^+ (^3A'') + S$	95.1	95.1	101.3		
1 → $S_2O^+ + H$	99.6	101.1	102.1		
1 → $OH^+ + S_2$	154.0	151.8	157.8		
1 → $H^+ + S_2O$[b]	173.3	173.3	171.8		
3 → $SH^+ + SO$	76.9	76.6	81.5		
3 → $SO^+ + SH$	79.1	77.0	81.8		
5 → $HSO^+ (^1A') + S$[c]	68.9	66.6	70.3		
$S_2^+ + H_2O$ → **1** + H	46.1	46.4	44.1		
$S_2 + H_2O^+$ → **1** + H	-24.2	-26.6	-30.3		

[a] The dissociation products are all considered in their ground state. [b] 173.0 kcal mol^{-1} (G3(MP2B3)) and 172.9 kcal mol^{-1} (G3), see text. [c] The singlet−triplet difference of 26.4 kcal mol^{-1} has to be added to ΔH.[28]

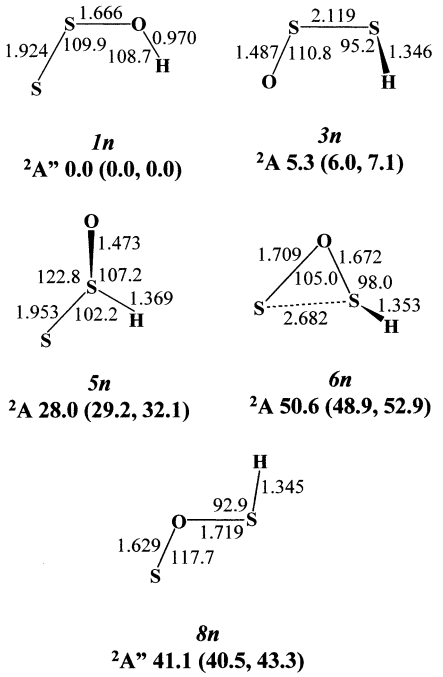

1n **^{2}A" 0.0 (0.0, 0.0)**

3n **^{2}A 5.3 (6.0, 7.1)**

5n **^{2}A 28.0 (29.2, 32.1)**

6n **^{2}A 50.6 (48.9, 52.9)**

8n **^{2}A" 41.1 (40.5, 43.3)**

Figure 2. B3LYP optimized geometries and relative energies (kcal mol^{-1}) at 298 K of [S_2OH] species, shown in parentheses are CCSD-(T) and CBS-Q relative energies.

even more prohibitive barriers separate $SSOH^+$ from the ring species **6** and **7** (66 kcal mol^{-1}) and $SOSH^+$ isomers (82 kcal mol^{-1}). Finally, two nonplanar species of SSOH and HSSO connectivity, ^{3}**1** and ^{3}**3**, were located on the triplet surface.

[S_2OH]. The most stable radical is the cis SSOH **1n** (Figure 2). The optimized geometry and the charge analysis suggest a bond order of 1.5 for the S−S bond. The unpaired electron is distributed on the two sulfur atoms. The corresponding trans isomer, less stable by 1.7 kcal mol^{-1}, shows a small imaginary frequency (92.1 cm^{-1}) and is not considered any further. The HSSO radical **3n** is a nonplanar species where the unpaired electron is distributed on the oxygen and central sulfur atoms, suggesting a bond order of 1.5 for the S−O bond. At the B3LYP level, we found a trans planar HSSO species only 0.7 kcal mol^{-1} above **3n**, which shows a very small vibrational frequency of 30.2 cm^{-1}. The barrier for the isomerization of this species to **3n** is as low as 0.03 kcal mol^{-1} at the B3LYP and CCSD(T) levels and disappears once we include the zero-point energy correction. For this reason, this species will not be considered any further. SSOH **1n** isomerizes to HSSO **3n** by overcoming a barrier of 28.6 kcal mol^{-1}, lying below the lowest dissociations of SSOH and of HSSO (Table 2). At higher energy, two nonplanar species were located as follows: **5n** of HS(S)O connectivity and **6n** having a pseudo-cyclic SOS unit. The cis conformer of SOSH connectivity shows an imaginary frequency at both the CBS-Q and MP2 levels, and only the trans **8n** conformer is reported in Figure 2.

TABLE 2: Energy Changes and Barrier Heights (kcal mol^{-1}, 298 K) Computed at the B3LYP/aug-cc-pVTZ+d, CCSD(T)/aug-cc-pVTZ+d, and CBS-Q Levels of Theory for Selected Dissociation and Isomerization Processes of S_2OH and S_2OH^-

	ΔH^a			barrier height	
process	B3LYP	CCSD(T)	CBS-Q	B3LYP	CCSD(T)
		S_2OH			
1n → **3n**	5.3	6.0	7.1	29.9	28.6
3n → **5n**	22.7	23.2	25.0	33.7	33.1
1n → $S_2 + OH$	50.0	51.2	55.4		
1n → $S_2O + H$	58.9	55.8	56.1	59.9	58.5
1n → $SOH (^2A'') + S$	77.0	74.1	81.3		
3n → $SO + SH$	40.6	40.4	44.4		
5n → $HSO (^2A'') + S$	44.5	42.3	43.5		
		S_2OH^-			
1a → **3a**	5.8	7.2	8.9	26.4	24.9
3a → **5a**	-1.3	-2.4	-5.0	21.5	21.2
^{3}**1a** → ^{3}**3a**	-4.2	-5.8		27.5	22.7
1a → $S_2O^- (^2A') + H$	50.7	53.7	51.4		
1a → $S_2^- (^2\Pi_g) + OH$	52.1	55.6	57.7		
1a → $S^- + SOH (^2A'')$	66.8	70.4	74.5		
1a → $SOH^- (^1A') + S$[b]	80.2	78.9	84.5		
3a → $SO^- (^2\Pi) + SH$	53.2	56.6	56.3		
5a → $S^- + HSO (^2A'')$	57.9	63.0	65.0		
5a → $HSO^- (^1A') + S$[b]	79.6	79.3	85.5		
^{3}**1a** → $OH^- (^1\Sigma^+) + S_2$	27.4	23.0			
^{3}**3a** → $SH^- (^1\Sigma^+) + SO$	15.9	12.5			

[a] The dissociation products are all considered in their ground state. [b] The singlet−triplet difference of 26.4 kcal mol^{-1} has to be added to ΔH.[28]

[S_2OH]$^-$. The most stable anion is the $SSOH^-$ ion **1a**, having an almost cis conformation, whereas $HSSO^-$ **3a** and $HS(S)O^-$ **5a** are nonplanar species (Figure 3). All bonds of the anions **1a**, **3a**, and **5a** can be classified as single bonds. The negative charge is mainly localized on the end-sulfur atom of **1a** and the oxygen atom of **3a**, respectively. In $HS(S)O^-$ **5a**, the negative charge is distributed on the oxygen and end-sulfur atoms, whereas the central sulfur atom carries a significant positive charge (+0.53 e). At higher energy, we found the species **7a** with a central oxygen atom and two $SOSH^-$ anions of the trans and pseudo-cis conformations, **8a** and **9a**. Finally, on the triplet surface, we located two cis planar species, ^{3}**1a** and ^{3}**3a**, of SSOH and HSSO connectivity, respectively.

Proton Affinity (PA) of S_2O. The S_2O molecule has three sites of different proton affinity, whose protonation yields $SSOH^+$, $HSSO^+$, and $HS(S)O^+$ ions. The most basic site is the oxygen atom; the end and central sulfur atoms have PA values lower by 10 and 38 kcal mol^{-1}, respectively (Figure 1). Very close PA values were obtained at the B3LYP, CCSD(T), and CBS-Q levels of theory (173.3−171.8 kcal mol^{-1}, see Table 1). Similar values, 173.0 and 172.9 kcal mol^{-1}, were obtained at the G3-(MP2B3) and G3 levels of theory usually utilized for PA

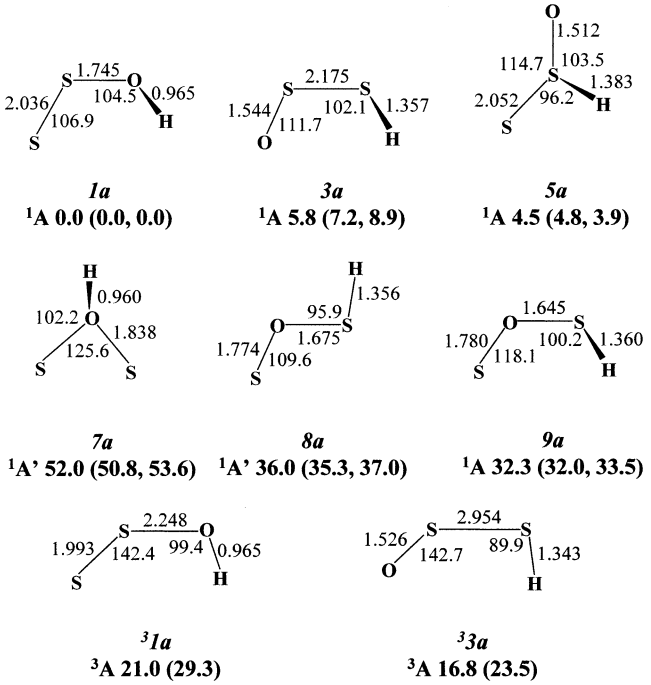

Figure 3. B3LYP optimized geometries and relative energies (kcal mol^{-1}) at 298 K of $[S_2OH]^-$ ions, shown in parentheses are CCSD(T) and CBS-Q relative energies.

calculations.[29] To further check the results, we computed the PA of H_2S and SO_2. We obtained 169.3 kcal mol^{-1} (H_2S) and 152.5 kcal mol^{-1} (SO_2) at the G3(MP2B3) level. The PA of H_2S agrees well with the experimental value of 168.5 kcal mol^{-1},[23a] and the PA of SO_2 agrees with the experimental value of 150.9 kcal mol^{-1} obtained by Szulejko and McMahon,[30] whereas it is quite different from the value of 160.7 kcal mol^{-1} reported in the NIST database.[23a] The PA of SO_2 was then computed at different levels of theory, obtaining again closely similar values: 153.2 (B3LYP), 153.1 (CCSD(T)), and 151.0 kcal mol^{-1} (CBS-Q). The computed PA of the electron-rich S_2O, 173.3 kcal mol^{-1}, appears satisfactorily in line with the PA of SO_2 and O_3. Notably, the experimentally derived PA of O_3 (148.0 kcal mol^{-1})[31a] is anchored to the PA of SO_2 taken as 150.9 kcal mol^{-1}, and it is in good agreement with the theoretical value obtained by Schaefer et al. (149.5 kcal mol^{-1}).[31b]

Formation and Analysis of the $[S_2OH]^+$ Ion. $[S_2OH]^+$ was obtained by protonation of S_2O from Brönstead acids AH^+, utilizing H_2, CH_4, C_2H_6, and CF_3COOH as reagent gases under chemical ionization (CI) conditions.

$$S_2O + AH^+ \rightarrow [S_2OH]^+ + A \quad (1)$$

$AH^+ = H_3^+$ (H_2/CI), CH_5^+ and $C_2H_5^+$ (CH_4/CI), $C_2H_5^+$ (C_2H_6/CI), $CF_3COOH_2^+$ (CF_3COOH/CI)

Variable amounts of SO_2 and H_2O were present in the CI plasma, since S_2O is unstable and difficult to prepare with high purity.[12]

The $[S_2OH]^+$ ions were structurally analyzed by CAD mass spectrometry[32] under high-resolution conditions, to separate $[S_2OH]^+$ from isobaric peaks. The spectra, reported in Table 3 (entries 1−4), were recorded in the TOF sector of the instrument at 0.8 keV collision energy. They display S_2^+ (*m*/*z* 64) as the most abundant fragment, together with S_2O^+ (*m*/*z* 80), SOH^+ (*m*/*z* 49), SO^+ (*m*/*z* 48), SH^+ (*m*/*z* 33), and S^+ (*m*/*z* 32). S_2^+ and SOH^+ can be traced to the dissociation of $SSOH^+$; SO^+ and SH^+ can be traced to the dissociation of $HSSO^+$. The CAD spectra are quite similar with the exception of that obtained by H_2/CI (first entry). The differences show that a mixture enriched by $HSSO^+$ is formed by H_2/CI as follows: the *m*/*z* 49/48 (SOH^+/SO^+) ratio decreases by a factor of 3.9 and the *m*/*z* 33 fragment (SH^+) increases by a factor of ≈3 (e.g., compared with entry 4).

From the computed PA of S_2O (173.3 kcal mol^{-1}) and the known PA values of the bases utilized in reaction 1,[23a] one can approximately evaluate $\Delta H° = -72.4$ kcal mol^{-1} ($A = H_2$), −43.4 kcal mol^{-1} ($A = CH_4$), −10.7 kcal mol^{-1} ($A = C_2H_4$), and −3.2 kcal mol^{-1} ($A = CF_3COOH$). In agreement, the experimental evidence shows that S_2O is protonated by H_3^+ on both the oxygen and the end-sulfur atoms giving $SSOH^+$ and $HSSO^+$ ions.[33] Conversely, a population of $SSOH^+$ ions is obtained by C_2H_6/CI and CF_3COOH/CI, although a selective protonation on the oxygen atom cannot be expected. Vibrationally excited reactants are able indeed to protonate the end-sulfur atom, less basic than oxygen by only 10 kcal mol^{-1}. A signature of this process is the presence of a fraction, though small, of SO_2H^+ and H_3O^+ ions (PA H_2O = 165 kcal mol^{-1}).[23a] A mixture enriched by $SSOH^+$ ions is also obtained by CH_4/CI that gives a quite similar CAD spectrum, likely because of mild protonation channels from abundant $C_2H_5^+$ and SO_2H^+ ions. The outlined picture thus indicates that the majority of the ions generated under these conditions have the $SSOH^+$ structure, whereas a mixture enriched by $HSSO^+$ ions is obtained by the most exothermic process.

A different and effective preparation of $[S_2OH]^+$ is illustrated in Figure 4. $[S_2OH]^+$ (*m*/*z* 81) was generated by chemical ionization of a gaseous mixture containing elemental sulfur and H_2O (Figure 4A). This route allows one to utilize isotopically labeled reactants, namely, elemental ^{34}S and $H_2{}^{18}O$. Ions at *m*/*z* 83 ($S_2{}^{18}OH^+$), 85 ($^{34}S_2OH^+$), and 87 ($^{34}S_2{}^{18}OH^+$) were obtained

TABLE 3: CAD Spectra of $[S_2OH]^+$ Ions

system		*m*/*z* (% Σ)[a]					
0.8 keV	S_2O/H_2 CI	*80* (9.6)	*64* (48.0)	*49* (13.8)	*48* (13.8)	*33* (6.5)	*32* (8.3)
	S_2O/CH_4 CI	*80* (8.8)	*64* (43.6)	*49* (23.1)	*48* (9.6)	*33* (3.5)	*32* (11.4)
	S_2O/C_2H_6 CI	*80* (7.9)	*64* (52.3)	*49* (21.8)	*48* (6.0)	*33* (1.8)	*32* (10.2)
	S_2O/CF_3COOH CI	*80* (9.1)	*64* (45.7)	*49* (26.3)	*48* (6.8)	*33* (2.3)	*32* (9.8)
	el-S/H_2O CI	*80* (9.2)	*64* (46.2)	*49* (25.1)	*48* (7.3)	*33* (2.5)	*32* (9.7)
	HgS/H_2O CI	*80* (9.1)	*64* (45.8)	*49* (24.2)	*48* (7.0)	*33* (2.4)	*32* (11.5)
	$^+NR^+$/CAD	*80* (7.4)	*64* (52.0)	*49* (9.5)	*48* (13.4)	*33* (6.5)	*32* (11.2)
8 keV	el-S/H_2O CI	*80* (8.8)	*64* (41.7)	*49* (21.5)	*48* (11.0)	*33* (≈4)[b]	*32* (12.8)
	HgS/H_2O CI	*80* (8.6)	*64* (42.2)	*49* (21.3)	*48* (10.9)	*33* (≈4)[b]	*32* (13.0)

[a] Uncertainty ±10%. [b] Unresolved peak.

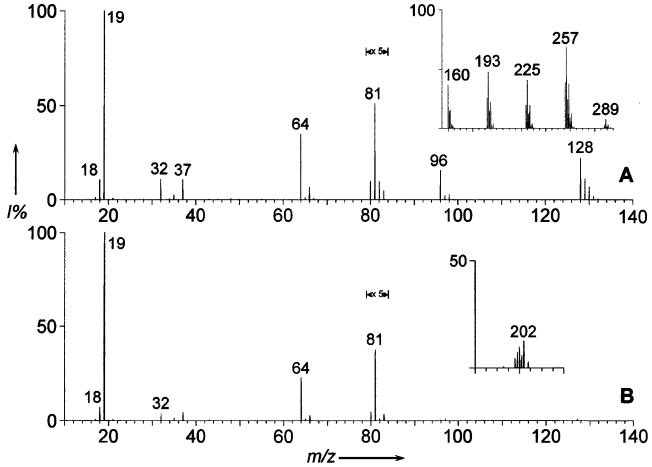

Figure 4. CI spectra of (A) el-S/H_2O and (B) HgS/H_2O mixtures. The insets display the high mass ranges: (A) S_n^+ and S_nH^+ ($n = 5-9$) ions and (B) Hg^+ multiplet.

by CI of various mixtures of labeled and unlabeled compounds, which ruled out isobaric contaminations.

Alternatively, a mixture of HgS and water was utilized (Figure 4B). While several S_n ($n = 2-12$) allotropes can be found in the vapor produced by heating elemental sulfur, depending on the pressure and temperature, it has been shown that S_2 accounts for about 90% of the sulfur species in the vapor produced by decomposition of HgS.[34] Consistent with this, S_2^+ is the most significant S_n^+ ion observed in the CI spectrum, showing that $[S_2OH]^+$ ions at *m*/*z* 81 are effectively formed under these conditions as well.

Accordingly, a conceivable route to $[S_2OH]^+$ in both the el-S/H_2O and HgS/H_2O mixtures is the following reaction (eq 2). Reactions of higher $S_n^{+/0}$ reactants ($n > 2$) can be in fact disregarded, since $[S_2OH]^+$ is effectively formed even in HgS/H_2O CI (Figure 4B).

$$S_2^{(+/0)} + H_2O^{(0/+)} \rightarrow [S_2OH]^+ + H \qquad (2)$$

The reaction of S_2^+ and H_2O is computed to be endothermic by 44.1 kcal mol^{-1} (CBS-Q) with respect to the formation of the most stable ion $SSOH^+$ **1**. This is consistent with earlier studies reporting that thermally relaxed S_2^+ is unreactive with H_2O.[35] However, thermal conditions are unlikely in our experiments and low-lying electronically excited states (i.e., $S_2^+(^4\Pi_u)$) are known to be also formed by electron impact of S_2, although their lifetime is not known.[34c,36] It must be noted that, to detect the $[S_2OH]^+$ ion, one has to work with a large excess of water which causes extensive self-protonation by H_2O^+. The reaction 2 of H_2O^+ and S_2 is computed to be exothermic by 30.3 kcal mol^{-1} with respect to the formation of **1** (CBS-Q), in such case the charge exchange to S_2 is expected to be a competing process though the efficiency is not known.

The structural analysis shows that the ionic population produced by el-S(HgS)/H_2O CI is identical to that produced by the mildest protonation of S_2O (Table 3). Thanks to the absence of isobaric contaminations, the spectra were recorded in different regions of the instrument and at different collision energies, namely, in the second field-free region at 8 keV (parts A and B of Figure 5) and in the TOF sector at 0.8 keV (Figure 5C). For comparison purposes, the latter were recorded under the same resolution conditions utilized for the $[S_2OH]^+$ ions from reaction 1. Importantly, the CAD spectra recorded at 8 and 0.8 keV show very limited differences despite the different lifetime and

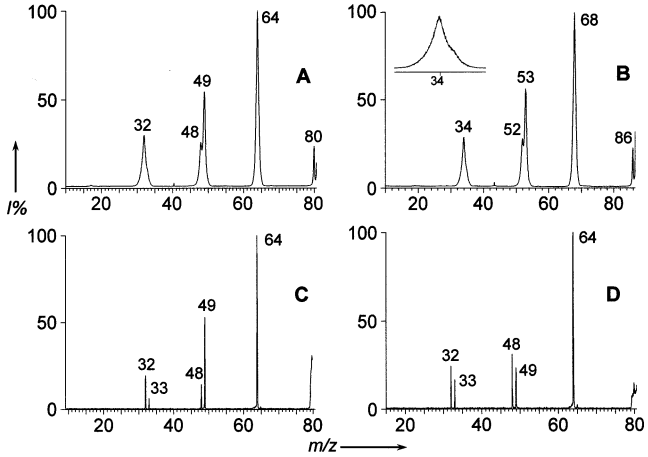

Figure 5. CAD spectra of (A) $[S_2OH]^+$ (*m*/*z* 81) from el-S/H_2O CI (8 keV collision energy) and (B) $[^{34}S_2{}^{18}OH]^+$ (*m*/*z* 87) from $^{34}S/H_2{}^{18}O$ CI (8 keV collision energy). The inset shows the unresolved peaks at *m*/*z* 34 and 35, corresponding to $^{34}S^+$ and $^{34}SH^+$. (C) CAD/TOF spectrum of $[S_2OH]^+$ (*m*/*z* 81) from el-S/H_2O CI (0.8 keV collision energy) and (D) NR-CAD spectrum of the $[S_2OH]^+$ recovery peak from $^+NR^+$.

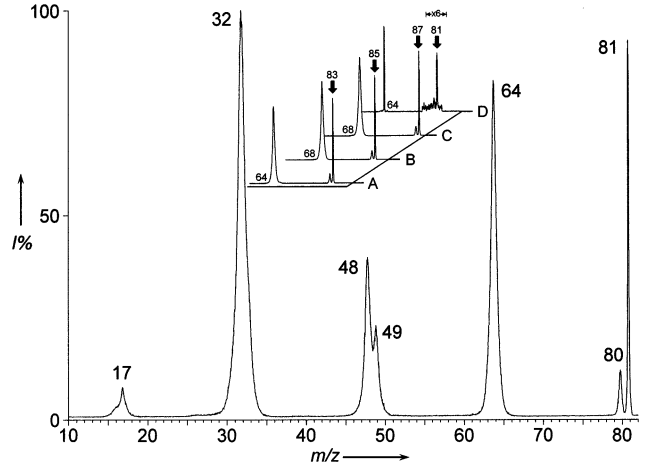

Figure 6. $^+NR^+$ spectrum of $[S_2OH]^+$ (*m*/*z* 81). Partial $^+NR^+$ spectra of $[S_2{}^{18}OH]^+$ (inset A), $[^{34}S_2OH]^+$ (inset B), and $[^{34}S_2{}^{18}OH]^+$ (inset C) showing the recovery peaks at *m*/*z* 83, 85, and 87. Inset D shows the partial $^+NR^+$ spectrum of $[S_2OH]^+$ (*m*/*z* 81) recorded at 0.8 keV.

collision energy. In summary, the experimental evidence provides the following most significant results:

(1) The analysis of the $[S_2OH]^+$ ions from reaction 1 discloses two distinctive fragmentation patterns, the one typical of mixtures enriched by $SSOH^+$ ions ($CH_4-C_2H_6-CF_3COOH$/CI of S_2O) and the other one taken as a signature of $HSSO^+$ ions (H_2/CI of S_2O).

(2) The $[S_2OH]^+$ ions obtained by el-S(HgS)/H_2O CI display the fragmentation pattern typical of mixtures enriched by $SSOH^+$ ions.

(3) This pattern does not change passing from 0.8 and 8 keV, which means that *no equilibration or change of composition* occurs due to collisional activation.

Formation and Analysis of SSOH and HSSO. It is recommendable in NR experiments to prepare the precursor ion in the absence of isobaric contaminations. Although the contribution of $^{33}SSO^+$ and $S_2{}^{17}O^+$ to $[S_2OH]^+$ is very small, we rigorously submitted to the NR process only the $[S_2OH]^+$ ions formed by el-S(HgS)/H_2O CI in the absence of S_2O.

Figure 6 reports the 8 keV $^+NR^+$ spectra of S_2OH^+, $S_2{}^{18}OH^+$, $^{34}S_2OH^+$, and $^{34}S_2{}^{18}OH^+$. They exhibit very intense recovery peaks (25% Σ) at the same masses as the precursor

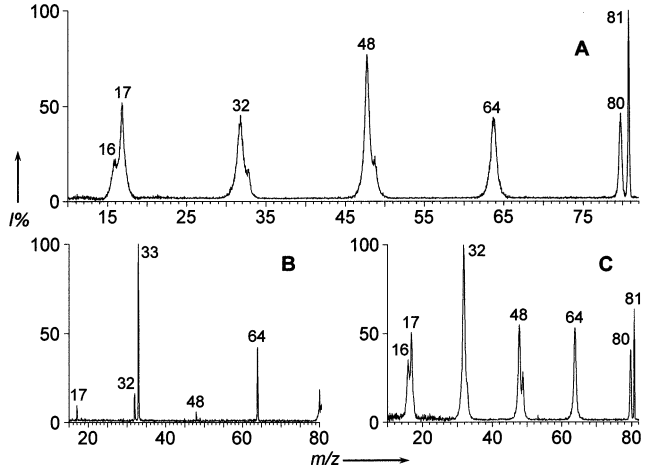

Figure 7. (A) $^{+}NR^{-}$ spectrum of $[S_2OH]^{+}$ (*m*/*z* 81), (B) NR-CAD mass spectrum of the $[S_2OH]^{-}$ recovery peak from $^{+}NR^{-}$, and (C) $^{+}CR^{-}$ spectrum of $[S_2OH]^{+}$ (*m*/*z* 81).

ions, *m*/*z* 81, 83, 85, and 87. Despite the fact that the $^{+}NR^{-}$ process is generally less efficient than $^{+}NR^{+}$, intense recovery peaks are found also in the $^{+}NR^{-}$ spectra (Figure 7A). All these findings prove the existence of $[S_2OH]$ gaseous species that survive for the maximum observation time available to the experiment, which is the time necessary to travel from the first to the second collision cell. This time window sets the lower limit of the neutral lifetime, that is, ≥ 0.8 μs for a species travelling at 8 keV and having a molecular weight of 87 Da. $^{+}NR^{+}$ experiments performed at low collision energy allowed us to increase the observation time up to 1.9 μs (inset D of Figure 6). Finally, the $^{+}NR^{-}$ experiments specifically identify the $[S_2OH]$ radical as a species of high electron affinity and also prove the existence of the $[S_2OH]^{-}$ anion.

The vertical nature of the NR processes at 8 keV provides indirect structural information on the detected neutrals, as these processes reasonably involve neutrals and ions of the same structure. Accordingly, the SSOH radical is very likely to be formed because the largest part of the ions submitted to the vertical neutralization has the $SSOH^{+}$ structure. Of course, the neutralization of a minor fraction of $HSSO^{+}$ ions possibly present in the ion beam cannot be excluded. Notwithstanding, in this work, we have obtained direct information by reanalyzing the "recovery" peaks, namely, the $[S_2OH]^{+}$ and $[S_2OH]^{-}$ ions eventually formed by reionization of the survived $[S_2OH]$ neutral. These NR-CAD spectra are reported in Figures 5D and 7B, respectively.

As to the $^{+}NR^{+}$ recovery peak, the analysis allows one to compare the "starting" and "final" $[S_2OH]^{+}$ ionic populations (parts C and D of Figure 5). The comparison shows that significant changes occur during the NR process. Unlike the precursor ions, the "reionized" $[S_2OH]^{+}$ population is close to that obtained by H_2/CI of S_2O (see also Table 3), which denotes a larger amount of $HSSO^{+}$ after the NR process. In addition, the comparative analysis of the $^{+}NR^{-}$, $^{+}CR^{-}$, and $^{+}NR^{-}$-CAD spectra gives strong evidence for the HSSO radical (Figure 7). We will illustrate first the formation of SSOH and then the processes leading to HSSO in both $^{+}NR^{+}$ and $^{+}NR^{-}$ experiments.

SSOH Radical. Due to the low barrier for the cis−trans isomerization (6.9 kcal mol^{-1}), a mixture of cis and trans $SSOH^{+}$ ions **1** and **2** is submitted to neutralization. Only the cis form **1n** of the SSOH radical is predicted to be a stable minimum on the potential energy surface of S_2OH. Upon inspection of Figures 1 and 2, it may be seen that ion **1** and the radical **1n** have closely related structures. In agreement, a difference of only 6.0 kcal mol^{-1} is found between the computed adiabatic and vertical recombination energies of $SSOH^{+}$ **1** (Table 4, first entry). Such a difference plays a major role in the excitation energy of the neutral, which is crucial to the survival and detection of intact neutrals. A reasonably low-energy excess, 7.2 kcal mol^{-1}, is also predicted for the formation of the cis SSOH **1n** from the trans $SSOH^{+}$ ion **2**.

TABLE 4: Vertical Excitation Energies (CCSD(T)), kcal mol^{-1}) of $S_2OH^{0/+/-}$ Species at the Geometry of the $S_2OH^{+/0}$ Species in Parentheses

$SSOH^{0/+/-}$			$HSSO^{0/+/-}$		
to	from	energy	to	from	energy
1n	**(1)**	6.0	**3n**	**(3)**	5.6
1n	**(2)**	7.2	**3n**	**(4)**	5.2
1	**(1n)**	4.7	**3**	**(3n)**	17.3
2	**(1n)**	4.4	**4**	**(3n)**	16.5
1a	**(1n)**	6.8	**3a**	**(3n)**	3.4
1a	**(1)**	24.4	**3a**	**(3)**	24.8
1a	**(2)**	26.4	**3a**	**(4)**	25.0
^{3}**1**	**(1n)**	6.1	^{3}**3**	**(3n)**	7.9
^{3}**1a**	**(1n)**	23.1	^{3}**3a**	**(3n)**	32.1
^{3}**1a**	**(1)**	27.5	^{3}**3a**	**(3)**	41.3

Likewise, the reionization of SSOH **1n** to the $SSOH^{+}$ cations (**1**−**2**) and the $SSOH^{-}$ anion (**1a**) is characterized by low vertical excitation energy, 4.7 and 6.8 kcal mol^{-1}, respectively (Table 4, entries 3−5). Consistent with this, the NR-CAD spectra of the recovery peaks show that $SSOH^{+}$ and $SSOH^{-}$ ions are reformed by positive and negative reionization (Figures 5D and 7B). Both spectra show indeed the characteristic fragmentations into S_2^{+} and SOH^{+} and into S_2^{-} and OH^{-} (see also Tables 1 and 2 and the next paragraphs) and conclusively demonstrate the detection of SSOH.

The computed ionization energy (IE) and electron affinity (EA) of SSOH are 8.50 and 1.78 eV, respectively. Due to the presence of the sulfur atoms, not unexpectedly SSOH is much more stable than the analogue O_3H located in a very shallow well.[6] The lowest-energy dissociation, into S_2 and OH, is indeed endothermic by 51.2 kcal mol^{-1} (Table 2). Nonetheless, the OH^{+} peak in the $^{+}NR^{+}$ spectrum is indicative of the dissociation of SSOH into S_2 and OH and subsequent reionization of the fragments. OH^{+} is in fact absent in the CAD spectrum of the precursor ion and in the NR-CAD of the recovery peak, according to the relative energies of the exit channels for the cation and the neutral (Tables 1−2). Notably, a barrier of 28.6 kcal mol^{-1}, lower than dissociation, characterizes the isomerization of SSOH **1n** to HSSO **3n** that is described in the next section.

HSSO Radical. As anticipated, the "reionized" $[S_2OH]^{+}$ population proves to be a mixture significantly enriched by $HSSO^{+}$ ions with respect to the "starting" $[S_2OH]^{+}$ population (parts C and D of Figure 5). Moreover, the latter gives the same CAD spectra irrespective of the collision energy and ion lifetime (Table 3). As a consequence, such a change of the ion composition in $^{+}NR^{+}$ experiments does not occur at the ionic stage by mere collisional activation of the $[S_2OH]^{+}$ ion and has to be traced to the energy involved in the NR process.

We have previously shown that both the neutralization of $SSOH^{+}$ and reionization of SSOH are characterized by favorable Franck−Condon factors. If a minor fraction of $HSSO^{+}$ ions in the beam is considered, one notes that also HSSO **3n** is formed with low-energy excess (5.6−5.2 kcal mol^{-1}, Table 4 right column) whereas the $HSSO^{+}$ ions are reformed with higher energy excess (17.3 kcal mol^{-1}) compared with $SSOH^{+}$. Finally, the reionization to triplet ions $SSOH^{+}$ (^{3}**1**) and $HSSO^{+}$ (^{3}**3**) is

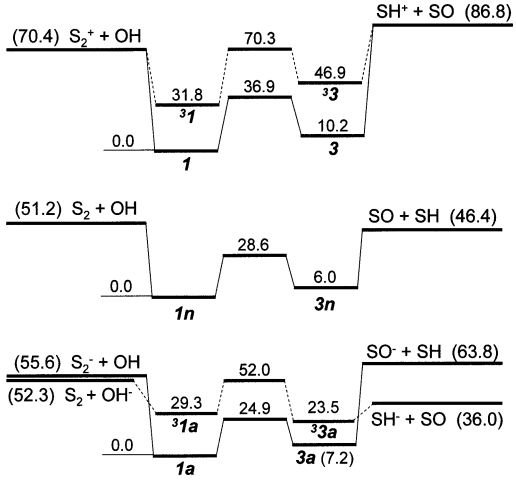

Figure 8. Simplified energy profiles relevant to the $SSOH^{+/0/-}$ and $HSSO^{+/0/-}$species ($\Delta H°$, kcal mol^{-1}, CCSD(T)).

also characterized by good Franck−Condon factors (Table 4). These vertical excitation energies represent the minimum internal energy deposited into neutrals and ions upon neutralization and reionization of ground-state species. Accordingly, if only relaxed species are considered, one cannot expect an enrichment of $HSSO^{+/0}$ nor a depletion of $SSOH^{+/0}$ species. The latter scenario is also very unlikely, not only on energetic grounds but also because such a depletion of the main part of the beam should definitely give lower recovery yields than observed.

The observed results rely on the distribution of internal energies occurring in the neutral population, as a result of the internal energy distribution of the precursor ion and the 8 keV collisional reduction. The experiments show indeed that a significant portion of neutrals survives the process, a minor fraction decomposes, and "non-decomposing" species have sufficient energy to isomerize during the microsecond time flight.[37] The **1n** → **3n** barrier (28.6 kcal mol^{-1}) exceeds the vertical excitation energy of **1n** by ca. 22 kcal mol^{-1} likely available to the hot fraction that isomerizes producing, in the absence of collisional relaxation, a mixture of SSOH and HSSO radicals.

The isomerization can be envisaged at the reionization stage as well, if the ions formed by the vertical oxidation of **1n** and **3n** have energy exceeding the **1** → **3** isomerization barrier (36.9 kcal mol^{-1}).[38] The reionization to the triplet ions ^{3}**1** and ^{3}**3** is not expected to play a significant role, as the dissociation into S_2^+ and OH competes at energies close to the isomerization barrier (Figure 8, Table 1). Notwithstanding, the ionic population detected after the NR process requires the intermediacy of HSSO, since the precursor ion population does not show this fragmentation pattern even under collisional activation.

Experiments involving negative reionization provide further confirming evidence for HSSO (Figure 7). Let us first compare the $^+$NR$^-$ spectrum and the NR-CAD spectrum of the recovery peak (parts A and B of Figure 7). The former displays superimposed neutral and ionic fragmentations whereas the latter displays only fragments from the dissociation of the *m*/*z* 81 reionized $[S_2OH]^-$ ion. Here the SH^- ion (*m*/*z* 33), traceable to $HSSO^-$, is the most abundant fragment (Figure 7B). Note that SO^- (*m*/*z* 48) is very small which indicates that $HSSO^-$ dissociates almost exclusively into SH^- (see the next paragraph). In contrast, the $^+$NR$^-$ spectrum shows SO^- as the most abundant fragment (Figure 7A). Although the comparison should take into account the different collision energies, this finding suggests a likely, albeit not exclusive, role of HSSO radicals.

Conclusive evidence for HSSO is given by a $^+$CR$^-$ experiment, where the two-electron reduction $[S_2OH]^+ \rightarrow [S_2OH]^-$ takes place (Figure 7C). It is well-known that different peak abundances in $^+$NR$^-$ and $^+$CR$^-$ spectra, recorded under the same conditions, are strongly indicative of processes traceable to the neutral intermediate.[39] Consistent with this, the SO^- abundance in the $^+$CR$^-$ spectrum amounts to 11% of the sum of all the ions, whereas it reaches 18% in the $^+$NR$^-$ spectrum. The result is particularly telling, because extensive fragmentation generally characterizes the $^+$CR$^-$ process, here also justified by the poor Franck−Condon overlap between the cation and anion surfaces (excitation energy of singlet and triplet $SSOH^-$ and $HSSO^-$ ions 25−40 kcal mol^{-1}, Table 4).

Formation and Analysis of the $[S_2OH]^-$ Anion. The $[S_2OH]^-$ anion generated in these experiments represents the conjugate base of the HSSOH acid, revealed in the gas phase by flash vacuum pyrolysis techniques.[5] HSSOH is an isomer of the thiosulfinic acids that have the HS(S)O skeletal, namely, HS(S)OH and HS(SH)O. The computed electron affinities of SSOH **1n** and HSSO **3n** amount to 1.78 and 1.73 eV, respectively, which explains the efficiency of the $^+$NR$^-$ process. Moreover, both the anions $SSOH^-$ **1a** and $HSSO^-$ **3a** can be formed with low excitation energy from the radicals **1n** and **3n** (6.8 and 3.4 kcal mol^{-1}, Table 4). Thus, the good overlap between the cation, neutral, and anion surfaces also accounts for the intense recovery peak detected in the $^+$NR$^-$ spectrum, which allows for further analysis of the reionized $[S_2OH]^-$ ions.

The ions forming the recovery peak are those $[S_2OH]^-$ ions not having sufficient energy to decompose in the time frame of the $^+$NR$^-$ experiment. Their NR-CAD spectrum (Figure 7B) displays the S_2^-/OH^- and SH^-/SO^- fragments, distinctive of $SSOH^-$ and $HSSO^-$ ions, respectively. Notably, the energy profile of Figure 8 shows that $SSOH^-$ ions may dissociate also by way of $HSSO^-$. The predominance of the SH^- fragment, with respect to SO^-, suggests in fact that the fragmentation occurs on the triplet surface, where the SH^- ($^1\Sigma^+$) + SO ($^3\Sigma$) products are formed by the lowest-energy channel (Table 2). The process most likely occurs by spin conversion along the dissociation path of the singlet $HSSO^-$ **3a** (Figure 8). Poor Franck−Condon factors feature indeed the reionization of SSOH and HSSO to the triplet anions ^{3}**1a** and ^{3}**3a** (Table 4), which are not expected to be a major part of the survived $[S_2OH]^-$ population. In agreement, the SOH^- fragment (*m*/*z* 49) is negligible in the NR-CAD spectrum of the reionized beam, consistent with the dissociation energies on the singlet surface where the S^- + SOH products are favored with respect to S + SOH^- (Table 2). Accordingly, the singlet $SSOH^-$ **1a** and $HSSO^-$ **3a** can be assigned to the survived population forming the recovery peak and subsequently analyzed by CAD.[40]

Conclusions

An experimental and computational study of $[S_2OH]$, $[S_2OH]^+$, and $[S_2OH]^-$ species was performed by mass spectrometric techniques and ab initio calculations. S_2O protonated on the end-sulfur and oxygen atoms has been prepared by chemical ionization mass spectrometry, and the PA has been computed at various levels of theory. SSOH has been prepared by collisional electron transfer to $SSOH^+$. It is characterized by an ionization energy of 8.50 eV, an electron affinity of 1.78 eV, an energy dissociation of 51 kcal mol^{-1} (into S_2 and OH), and a minimum lifetime of 1.9 μs. Experiments that demonstrate the isomerization of SSOH to HSSO are reported.

HSSO, less stable than SSOH by 6 kcal mol^{-1}, is characterized by an ionization energy of 8.68 eV, an electron affinity of 1.73 eV, and an energy dissociation of 40 kcal mol^{-1} (into SO and SH). $SSOH^-$ and $HSSO^-$, the conjugate bases of HSSOH, have been prepared by electron transfer to either $[S_2OH]$ or $[S_2OH]^+$.

Acknowledgment. This work has been financially supported by the Italian Government (PRIN-FIRB) and Rome University "La Sapienza". The helpful editorial assistance by Stefania Recaldin is gratefully acknowledged.

Supporting Information Available: Tables of energies and vibrational frequencies are given. This material is available free of charge via the Internet at http://pubs.acs.org.

References and Notes

(1) (a) Schurath, U.; Weber, M.; Becker, K. H. *J. Chem. Phys.* **1977**, *67*, 110. (b) Iraqi, M.; Goldberg, N.; Schwarz, H. *J. Phys. Chem.* **1994**, *98*, 2015. (c) Bowie, J. H.; Stringer, M. B.; Haynes, R. N. *Rapid Commun. Mass Spectrom.* **1990**, *4*, 129. (d) O'Hair, R. A. J.; DePuy, C. H.; Bierbaum, V. M. *J. Phys. Chem.* **1993**, *97*, 7955.

(2) (a) Decker, B. K.; Adams, N. G. *Int. J. Mass Spectrom. Ion Process.* **1997**, *165/166*, 257. (b) Decker, B. K.; Adams, N. G.; Babcock, L. M. *Int. J. Mass Spectrom.* **1999**, *185/186/187*, 727.

(3) (a) Block, E.; O'Connor, J. *J. Am. Chem. Soc.* **1974**, *96*, 3921. (b) Schmidt, H.; Steudel, R.; Sülzle, D.; Schwarz, H. *Inorg. Chem.* **1992**, *31*, 941.

(4) (a) de Petris, G.; Rosi, M.; Troiani, A. *Chem. Commun.* **2006**, 4416. (b) de Petris, G. *Acc. Chem. Res.* **2002**, *35*, 305. (c) Cacace, F.; Cipollini, R.; de Petris, G.; Rosi, M.; Troiani, A. *J. Am. Chem. Soc.* **2001**, *123*, 478. (d) Cacace, F.; de Petris, G.; Rosi, M.; Troiani, A. *Chem. Commun.* **2001**, 2086.

(5) Königshofen, A.; Behnke, M.; Hoverath, M.; Hahn, J. *Z. Anorg. Allg. Chem.* **1999**, *625*, 1779.

(6) (a) Cacace, F.; de Petris, G.; Pepi, F.; Troiani, A. *Science* **1999**, *285*, 81. (b) Dupuis, M.; Fitzgerald, G.; Hammond, B.; Lester, W. A.; Schaefer, H. F., III. *J. Chem. Phys.* **1986**, *84*, 2691. (c) Yu, H. G.; Varandas, A. J. C. *Chem. Phys. Lett.* **2001**, *334*, 173. (d) Fabian, W. M. F.; Kalcher, J.; Janoschek, R. *Theor. Chem. Acc.* **2005**, *114*, 182.

(7) (a) Frank, A. J.; Sadílek, M.; Ferrier, J. G.; Tureček, F. *J. Am. Chem. Soc.* **1996**, *118*, 11321. (b) Goumri, A.; Rocha, J.-D. R.; Laakso, D.; Smith, C. E.; Marshall, P. *J. Phys. Chem. A* **1999**, *103*, 11328. (c) Blitz, M. A.; Hughes, K. J.; Pilling, M. J.; Robertson, S. H. *J. Phys. Chem. A* **2006**, *110*, 2996. (d) Ballester, M. Y.; Varandas, A. J. C. *Chem. Phys. Lett.* **2007**, *433*, 279.

(8) (a) Hapke, B. *Icarus* **1989**, *79*, 56. (b) Na, C. Y.; Esposito, L. W. *Icarus* **1997**, *125*, 364. (c) Spencer, J. R.; Jessup, K. L.; McGrath, M. A.; Ballester, G. E.; Yelle, R. *Science* **2000**, *288*, 1208.

(9) Radi, P. P.; Mischler, B.; Schlegel, A.; Tzannis, A.-P.; Beaud, P.; Gerber, T. *Combust. Flame* **1999**, *118*, 301.

(10) Bernardi, F.; Cacace, F.; de Petris, G.; Pepi, F.; Rossi, I.; Troiani, A. *Chem.*−*Eur. J.* **2000**, *6*, 537.

(11) (a) Holmes, J. L. *Mass Spectrom. Rev.* **1989**, *8*, 513. (b) Schalley, C. A.; Hornung, G.; Schröder, D.; Schwarz, H. *Chem. Soc. Rev.* **1998**, *27*, 91. (c) Tureček, F. *Theory and Ion Chemistry, The Encyclopedia of Mass Spectrometry*; Armentrout, P. R., Ed.; Elsevier: New York, 2003; Vol. 1.

(12) Steudel, R. *Top. Curr. Chem.* **2003**, *231*, 203.

(13) (a) Becke, A. D. *J.Phys. Chem.* **1993**, *98*, 5648. (b) Stephens, P. J.; Devlin, F. J.; Chablowski, C. F.; Frisch, M. J. *J. Phys. Chem.* **1994**, *98*, 11623.

(14) Mannfors, B.; Koskinen, J. T.; Pietilä, L.-O.; Ahjopalo, L. *J. Mol. Struct.* **1997**, *393*, 39.

(15) Bauschlicher, C. W.; Ricca, A.; Partridge, H.; Langhoff, S. R. *Recent Advances in Density Functional Theory*; Chong, D. P., Ed.; World Scientific Publishing Co.: Singapore, 1997; Part II.

(16) (a) Bartlett, R. J. *Annu. Rev. Phys. Chem.* **1981**, *32*, 359. (b) Raghavachari, K.; Trucks, G. W.; Pople, J. A.; Head-Gordon, M. *Chem. Phys. Lett.* **1989**, *157*, 479. (c) Olsen, J.; Jorgensen, P.; Koch, H.; Balkova, A.; Bartlett, R. J. *J. Chem. Phys.* **1996**, *104*, 8007.

(17) Peng, C.; Schlegel, H. B. *Isr. J. Chem.* **1993**, *33*, 449.

(18) (a) Dunning, T. H. *J. Chem. Phys.* **1989**, *90*, 1007. (b) Woon, D. E.; Dunning, T. H. *J. Chem. Phys.* **1993**, *98*, 1358. (c) Kendall, R. A.; Dunning, T. H.; Harrison, R. J. *J. Chem. Phys.* **1992**, *96*, 6796.

(19) Bauschlicher, C. W., Jr.; Partridge, H. *Chem. Phys. Lett.* **1995**, *240*, 533.

(20) Wang, N. X.; Wilson, A. K. *J. Phys. Chem. A* **2005**, *109*, 7187.

(21) Azizi, Z.; Roos, B. O.; Veryazov, V. *Phys. Chem. Chem. Phys.* **2006**, *8*, 2727.

(22) Ochterski, J. W.; Petersson, G. A.; Montgomery, J. A., Jr. *J. Chem. Phys.* **1996**, *104*, 2598.

(23) (a) *NIST Chemistry WebBook, NIST Standard Reference Database Number 69*, Linstrom, P. J., Mallard, W. G., Eds.; National Institute of Standards and Technology: Gaithersburg, MD, 2005. (b) Lodders, K. *J. Phys. Chem. Ref. Data* **2004**, *33*, 357.

(24) (a) Gonzales, C.; Schlegel, H. B. *J. Chem. Phys.* **1989**, *90*, 2154. (b) Gonzales, C.; Schlegel, H. B. *J. Phys. Chem.* **1990**, *94*, 5523.

(25) (a) Flükiger, P.; Lüthi, H. P.; Portmann, S.; Weber, J. *MOLEKEL 4.3*; Swiss Center for Scientific Computing: Manno, Switzerland, 2000−2002. (b) Portmann, S.; Lüthi, H. P. *Chimia* **2000**, *54*, 766.

(26) Frisch, M. J.; et al. *Gaussian 03*, revision B.04; Gaussian, Inc.: Wallingford, CT, 2004.

(27) Davy, R. D.; Skoumbourdis, E. *Mol. Phys.* **1998**, *94*, 539.

(28) Sansonetti, J. E.; Martin, W. C.; Young, S. L. *Handbook of Basic Atomic Spectroscopic Data*; National Institute of Standards and Technology: Gaithersburg, MD, 2006.

(29) Curtiss, L. A.; Redfern, P. C.; Raghavachari, K.; Rassolov, V.; Pople, J. A. *J. Chem. Phys.* **1999**, *110*, 4703.

(30) Szulejko, J. E.; McMahon, T. B. *J. Am. Chem. Soc.* **1993**, *115*, 7839.

(31) (a) Cacace, F.; Speranza, M. *Science* **1994**, *265*, 208. (b) Meredith, C.; Quelch, G. E.; Schaefer, H. F., III. *J. Am. Chem. Soc.* **1991**, *113*, 1186.

(32) Cooks, R.G. *Collision Spectroscopy*; Plenum Press: New York, 1978.

(33) In principle, the less stable protomer $HS(S)O^+$ **5** could also be formed. However, the fragment distinctive of **5**, HSO^+, is an isomer of SOH^+ which prevents its definite identification. In addition, isomer **5** is formed quite close to the isomerization barrier to the most stable ion **4** (25.9 kcal mol^{-1}, Table 1).

(34) (a) Berkowitz, J. *Elemental Sulphur*; Meyer, B., Ed.; Meyer, Interscience: New York, 1965. (b) Meyer, B. *Chem. Rev.* **1976**, *76*, 367. (c) Berkowitz, J. *J. Chem. Phys.* **1975**, *62*, 4074.

(35) (a) Laudenslager, J. B.; Huntress, W. T. *Int. J. Mass Spectrom. Ion Phys.* **1974**, *14*, 435. (b) Niedner-Schatteburg, G.; Šilha, J.; Schindler, T.; Bondybey, V. E. *Chem. Phys. Lett.* **1991**, *187*, 60.

(36) (a) Dyke, J. M.; Golob, L.; Jonathan, N.; Morris, A. *J. Chem. Soc., Faraday Trans. 2* **1975**, *71*, 1026. (b) Rosinger, W.; Grade, M.; Hirschwald, W. *Int. J. Mass Spectrom. Ion Phys.* **1983**, *47*, 239.

(37) Examples of rearrangements occurring in NR processes can be found in the following: (a) Blanksby, S. J.; Schröder, D.; Dua, S.; Bowie, J. H.; Schwarz, H. *J. Am. Chem. Soc.* **2000**, *122*, 7105. (b) McAnoy, A. M.; Dua, S.; Schröder, D.; Bowie, J. H.; Schwarz, H. *J. Phys. Chem. A* **2004**, *108*, 2426. (c) McAnoy, A. M.; Bowie, J. H.; Dua, S. *J. Phys. Chem. A* **2004**, *108*, 3994.

(38) A major energy content is expected for the $HSSO^+$ ions **3** and **4**, formed from ground-state HSSO **3n** at energies close to their isomerization barrier (18 kcal mol^{-1}) and ca. 9 kcal mol^{-1} below the **1**→ **3** isomerization energy. The geometries of **3** (**4**) and **3n** and the energy distribution however ensure formation of $HSSO^+$ ions far below the **1** → **3** barrier. Indeed, neutrals **3n** having a low-energy excess of ca. 5 kcal mol^{-1} can be vertically oxidized to ground-state ions **3** and **4** (Table 4).

(39) Schalley, C. A.; Hornung, G.; Schröder, D.; Schwarz, H. *Int. J. Mass Spectrom. Ion Process.* **1997**, *172*, 181.

(40) A word is reserved for the $HS(S)O^-$ anion **5a**, which is slightly less stable than **1a**. The **1a** → **3a** and **3a** → **5a** isomerization barriers are comparable (Table 2); however, the fragmentation of **3a** by crossing the triplet surface could effectively compete with the isomerization to **5a**. More importantly, the fragmentation products distinctive of **5a** (e.g., S_2O^-, S^-) are common to all the other species, which prevents its identification.